# Verification of Cloud Cover Forecast with Satellite Observation over West Africa

Nathalie Söhne, Jean-Pierre Chaboureau, Françoise Guichard

# Verification of Cloud Cover Forecast with Satellite Observation over West Africa

NATHALIE SÖHNE AND JEAN-PIERRE CHABOUREAU

*Laboratoire d'Aérologie, Université de Toulouse, and CNRS, Toulouse, France*

FRANÇOISE GUICHARD

*GAME/CNRM, CNRS, and Météo-France, Toulouse, France*

(Manuscript received 19 October 2007, in final form 15 February 2008)

ABSTRACT

The 3-hourly brightness temperatures (BTs) at 10.8 $\mu$m from the Meteosat Second Generation (MSG) satellite were used to document the cloud system variability over West Africa in the summer of 2006 and to evaluate the quality of the Méso-NH model forecasts of cloud cover in the African Monsoon Multidisciplinary Analysis (AMMA) framework. Cloud systems were observed over the Guinean and Sahelian bands with more frequent occurrence and patchier structures in the afternoon. Some intraseasonal variations of the number of cloud systems were found, partly related to the intermittency of the African easterly wave (AEW) activity. Compared to the MSG observations, the Méso-NH model reproduces the overall variation of the BT at 10.8 $\mu$m well at $D + 1$ forecast. The model captures the BT diurnal cycle under conditions of clear-sky and high-cloud cover, but misses the lowest BT values associated with deep convection. Forecasted cloud systems are more numerous and smaller, hence patchier, than those observed. These results suggest some deficiencies in the model's convection and cloud parameterization schemes. The use of meteorological scores further documents the skill of the model to predict cloud systems. Beyond some systematic differences between simulations and observations, analysis also suggests that the model high-cloud forecast is improved under specific synoptic forcing conditions related to AEW activity. This indicates that room exists for improving the skills of weather forecasting over West Africa.

## 1. Introduction

Clouds and precipitation are sensible weather elements that are crucial to forecast in the tropics. Despite the importance of rain for human activities, skill in forecasting tropical rainfall events on a day-to-day basis has not been explored extensively, with the exception of tropical cyclones. This can be explained by the limited value of numerical weather prediction for forecasting weather involving convection because of the paucity of appropriate mesoscale observational data and the limitations of both current initialization procedures and physical parameterization (Smith et al. 2001). Thus, there has been more focus on the ability of the general circulation models (GCMs) to represent the broad characteristics of the tropical atmosphere. For example, a well-established deficiency in GCMs is the failure to capture the diurnal cycle of deep convection over land, both in magnitude and phase (e.g., Guichard et al. 2004). In particular, deep convection in GCMs tends to be in phase with low-level temperature and atmospheric instability. This results in a predicted onset of convective rainfall earlier than observed. Last, the mesoscale organization of convection poorly simulated by GCMs is also a strong issue, particularly for impact studies such as on the hydrologic cycle (Lebel et al. 2000). These features suggest fundamental shortcomings in the parameterization of the surface, radiative, boundary layer, cloud, and convective processes.

In the Sahel, a semiarid zonal band around 10°–18°N extending coherently across Africa, most of the precipitation arises from mesoscale convective systems (MCSs) during the Northern Hemisphere summer (e.g., Mathon et al. 2002). The correct prediction of MCSs is therefore of importance for human needs and has been identified as an objective of the African Monsoon Multidisciplinary Analysis (AMMA) research program

*Corresponding author address:* Dr. Jean-Pierre Chaboureau, Laboratoire d'Aérologie, Observatoire Midi-Pyrénées, 14 av. Belin, F-31400 Toulouse, France.
E-mail: jean-pierre.chaboureau@aero.obs-mip.fr

DOI: 10.1175/2008MWR2432.1

(Redelsperger et al. 2006). MCSs are characterized by a spatial extent of a few hundred kilometers and a duration from several hours up to a few days. They result from the scale interaction between different processes. MCSs are born as individual convective cells triggered with the daytime boundary layer development. Their further growth is influenced by the vertical shear associated with the African easterly jet (AEJ), a seasonal midlevel jet that results from the temperature meridional gradients over the continent. In addition, convective activity is significantly modulated by African easterly waves (AEWs; e.g., Reed et al. 1977; Diedhiou et al. 1999), although the nature of the relationships involved is still unclear. AEWs correspond to synoptic-scale disturbances with periods of a few days that have often been understood to result from instability of the AEJ (Burpee 1972). Recently, a new perspective has been afforded suggesting that the initiation and intermittence of AEWs is caused by pulsations of deep convection (Hsieh and Cook 2005; Hall et al. 2006). In any case, such strong interaction between the convective and synoptic scales makes MCSs difficult to forecast.

In consequence, skillful forecasting of MCSs first requires a correct representation of the surface, radiative, boundary layer, cloud, and convective processes. In large-scale models (e.g., with a grid spacing larger than 10 km), all these processes are parameterized, so the ability of a model to forecast MCSs is an important test of its physical parameterization schemes. In addition, some key processes specific to the Sahel need to be well represented. For example, soil moisture is characterized there by marked spatial and temporal variability that correlates with the path of afternoon convection via mechanisms that still need to be determined (Taylor and Ellis 2006). Dust plays an important role in the dynamics in the region via its radiative properties. Thus, a substantial weakening of the AEJ with the forecast range in the European Centre for Medium-Range Weather Forecasts (ECMWF) model has been partly attributed to an overestimated direct radiative forcing by dust aerosols (Tompkins et al. 2005). Furthermore, the use of prognostic dust aerosol, instead of climatology, in a regional model was found to better capture the observed convective activity at the 2-day range (Chaboureau et al. 2007b).

The forecast skill also depends on the initial conditions given in the models. West Africa, along with most of the continent, is a well-known data-sparse region with few routinely launched radiosondes. In consequence, the model analyses are strongly driven by the guess from the previous run and the few satellite data assimilated over land. During the AMMA special observing period (SOP), a considerable effort was made to ensure that all relevant data (e.g., from extra radiosondes, dropsondes, etc.) were broadcast to the Global Telecommunication System to support operational forecasting (Redelsperger et al. 2006). The use of RS80 A-Humicap radiosondes at some stations during the AMMA SOP yielded, however, dry bias in the moisture analysis in the vicinity of these stations that could reduce the forecast skill substantially (A. Agusti-Panareda and M. Nuret 2007, personal communication).

In addition to the different sources of errors that affect the forecast skill, a difficulty in estimating such skill in a systematic way arises from the source of the observation. As noted by Simmons and Hollingsworth (2002), verification of forecasts by comparison with radiosonde observations can give rise to difficulties in interpreting the verification statistics because of the variation over time in the number and type of stations reporting. It may be even more difficult with precipitation measurements from rain gauges, because of the marked patchiness of rainfall. An alternative to the terrestrial source of observations is provided by satellites with good coverage in time and space. In particular, the Meteosat Second Generation (MSG) satellite provides indirect information on cloud properties over Africa every 15 min. The observation of the earth's upwelling radiation is therefore employed to estimate rainfall products, but the unknown errors associated with such rain retrievals limit their value for evaluating the performance of forecasting models (e.g., Adler et al. 2001).

Here, we adopted a model-to-satellite approach, in which satellite brightness temperature (BT) images were directly compared to BTs computed from predicted model fields (Morcrette 1991). This approach offers the advantage that the satellite data are used in an objective way, without being combined with any ancillary data. It is especially powerful in identifying discrepancies of cloud cover forecasts (Chaboureau et al. 2000; Chevallier and Kelly 2002) and tuning critical parameters in cloud schemes (Chaboureau et al. 2002; Keil et al. 2006). Previous works have used the model-to-satellite approach on a long-term series of forecasts made by the Méso-NH model (Lafore et al. 1998) to test the impact of different parameterizations on the overall prediction of cloud cover (Chaboureau and Bechtold 2005), cirrus cover (Chaboureau and Pinty 2006), and convective overshoots (Chaboureau et al. 2007a). These studies have shown the value of the model-to-satellite approach in giving a specific constraint to the model.

The verification of the cloud cover forecast is carried out here by combining the model-to-satellite approach with the calculation of scores. This is applied for the first time to a series of daily 48-h forecasts made with

the Meso-NH model during a 1-month period, from 23 July to 22 August 2006, covering the AMMA SOP 2a2. We use the BT at 10.8 $\mu$m from 3-hourly MSG observations as it is mainly affected by cloud-top heights. The method described here provides a framework for assessing the cloud cover forecast and the impact of forthcoming improvements to the representation of clouds in the model. Within the specific focus of the present study, the monsoon season over West Africa, cloud cover forecasts are expected to be closely related to simulated moist convective features.

The paper is organized as follows. Section 2 presents the Méso-NH model and the way the model forecasts are compared to satellite observations. Section 3 provides an analysis of the high-cloud cover variability over the 1-month period. Section 4 describes the diurnal variability and points out some deficiencies in the cloud parameterizations. Section 5 discusses the synoptic variability of the high-cloud cover and the increase of the forecast skill with AEW activity. Section 6 concludes the study.

## 2. Model and satellite observations

The Méso-NH model (Lafore et al. 1998) was adopted as a nonhydrostatic regional model with the same configuration as used by Chaboureau et al. (2007b). Vertical grid spacing in the free troposphere was set to 600 m, with horizontal grid spacing of 32 km. The model includes a 1.5-order turbulence scheme, interactive radiation, a dust scheme, and a prognostic microphysical scheme including the three water phases with five species of precipitating and nonprecipitating liquid and solid water (Pinty and Jabouille 1998), and a modified ice-to-snow autoconversion parameterization following Chaboureau and Pinty (2006). Deep and shallow convective transport and precipitation are parameterized following Bechtold et al. (2001) based on the work of Kain and Fritsch (1993). Subgrid cloud cover and condensate content are parameterized as a function of the normalized saturation deficit by taking into account both turbulent and convective contributions (Chaboureau and Bechtold 2002, 2005).

From 23 July to 22 August 2006, a total of 31 daily 48-h forecasts were run over a domain of 3840 km $\times$ 2880 km covering West Africa. In addition to the classical meteorological outputs, dust (as in Chaboureau et al. 2007b), lightning $NO_x$ (as in Mari et al. 2006), and a tracer to mimic soil emission by volatile organic components were forecasted to offer guidance to the operation flight plan during the SOP 2a2. The simulation domain and its associated topography are shown in Fig. 1. The individual forecasts were initialized with 12-h ECMWF forecasts based on the 1200 UTC ECMWF analyses. The choice of 12-h forecasts, rather than the analyses, for the initialization was dictated by the need to have forecasts in time for the morning briefing. The initial and boundary conditions of the numerical experiments were provided for the horizontal wind, the temperature, and the water vapor. The lateral boundaries were taken 6-hourly from the ECMWF forecasts. Clouds were initialized to zero values, so the mixing ratios of the liquid and ice water species built up during the course of the simulations.

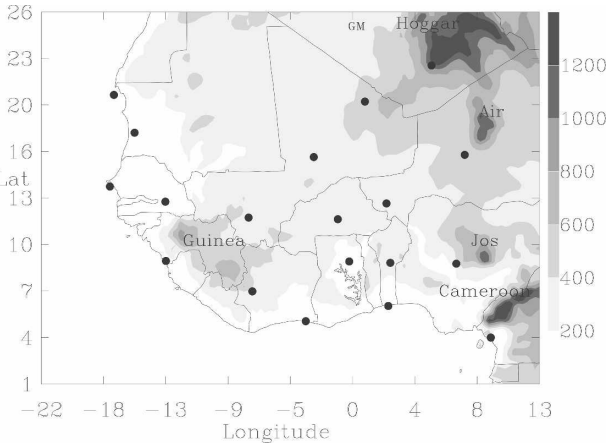


FIG. 1. Topography (m) of the simulation domain. The dots show the locations of soundings performed during the SOP.

The BTs corresponding to the MSG observations were computed using the Radiative Transfer for Television and Infrared Observation Satellite (TIROS) Operational Vertical Sounder (RTTOV) code version 8.7 (Saunders et al. 2005). The surface emissivity was given by the Moderate Resolution Imaging Spectroradiometer (MODIS) MYD11C3 product. The computed BTs at 10.8 $\mu$m were compared to MSG observations every 3 h. As the latter have a 2.5-km horizontal resolution at the nadir, the observed radiances were averaged and projected onto the Méso-NH grid, then converted to BTs.

The BTs at 10.8 $\mu$m were used to characterize the cloud patchiness. Cloud systems (clear-sky areas) were defined as groups of adjacent grid points with BT lower (higher) than a threshold value. The number of resulting cloud systems and clear-sky areas divided by the number of grid points defined the patchiness (Schröder et al. 2006). The BTs were also used to verify the cloud cover forecasts. Here we use categorical scores that measure the correspondence between simulated and observed occurrence of events at grid points. They were first developed to focus on tornado detection (Finley 1884) and later on to verify the occurrence of high pre-

cipitation rates (e.g., Ebert et al. 2003). For a given threshold, a contingency table is constructed using that threshold to distinguish nonhigh-cloud from high-cloud events in the observation and the forecast. Following the convention used by Wilks (1995), this gives the correct prediction of high clouds ($a$ or hits), the events not observed ($b$ or false alarm), the observed high-clouds not forecasted ($c$ or missing alarm), and the correct forecasts of nonevents when there were no high clouds ($d$ or hit nonactive). In the following, we use the probability of detection [POD; $a/(a + c)$], the false alarm ratio [FAR; $b/(a + b)$], and the Heidke skill score [HSS; $(a + d - h_r)/(a + b + c + d - h_r)$]. The POD gives the hits of events that were correctly forecast, the FAR is the fraction of events that did not occur, and the HSS measures the fraction of correct forecasts after eliminating those that would be correct because of chance $\{h_r = [(a + c)\ (a + b) + (d + c)\ (d + b)]/(a + b + c + d)\}$. Such scores quantify the ability of the model to forecast an event at the right place. They have been employed to verify the realism of the model-generated BTs against satellite-observed BTs in the infrared and microwave ranges for midlatitude case studies (Söhne et al. 2006; Chaboureau et al. 2008).

The score calculation made by comparing grid point with grid point can lead to the double penalty effect. This arises when an observed feature of few grid points is realistically forecast but is misplaced. A model is penalized twice, once for missing the actual feature and again for forecasting it where it is not. The double penalty effect can be misleading by eliminating efficiently valuable information on small-scale features from the model skill. Therefore, scores were also calculated by comparing fractions of occurrence of events over a sized area. Such a calculation was applied to all the scores defined above using a threshold set at 50%. Thus, the forecasts and the observations were remapped over larger areas where high-cloud events corresponded to more than 50% of cloudy grid points. In addition, the Fractions skill score (FSS) is a variation of the Brier score in which fractions (considered as probabilities) are compared with fractions (Roberts and Lean 2008). The FSS has a range from 0 (zero skill) to 1 (perfect skill). To estimate the current FSS against uniform forecasts, we used two basic FSS measures, namely $\mathrm{FSS}_{\mathrm{random}}$ and $\mathrm{FSS}_{\mathrm{uniform}}$. $\mathrm{FSS}_{\mathrm{random}}$ denotes the FSS that would be obtained from a random forecast with the same fractional coverage over the domain as that of the high-cloud cover ($f_0$), while $\mathrm{FSS}_{\mathrm{uniform}}$ represents the FSS that would be obtained at the grid scale with a fraction equal to $f_0$ at every grid point (Roberts and Lean 2008). The areas used here are squares of up to 7 by 7 grid points (i.e., areas of 224 km by 224 km).

## 3. Cloud system variability

A typical situation in summer over West Africa is illustrated at 1200 UTC 14 August 2006 (Fig. 2, top). Two major convective systems were observed over Niger and the Guinea Highlands as seen with BTs of less than 230 K spanning a few hundred kilometers squared. Smaller convective systems were also present over the Jos Plateau and the Cameroon Highlands. The BTs in the range of 260–290 K mostly occurred off the African coasts and at low latitudes (less than 15°N). They resulted from either low-level clouds or thin cirrus detrained from the nearby convection. The BTs larger than 290 K over the Sahara and the ocean corresponded to almost-clear-sky areas. The 36-h forecast represents the overall BT variability reasonably well (Fig. 2b). In particular, the two major convective systems were predicted but too far south and with too narrow an extent of low BT values. The smaller-sized systems are also present but less developed than in the observations.

Note that the 12-h forecast (not shown) for that date missed the system over Niger. This drawback occurred quite often, and is not completely surprising, given the use of a cold start (i.e., clear-sky initial conditions) together with the characteristic space and time scales of MCS, which can be much larger than a few hours. In addition, it seems likely that the initial fields do not properly capture mesoscale structures associated with MCSs, such as convective outflows that may act as convective triggers in an otherwise convection inhibiting environment as typically encountered by squall lines in the Sahel (e.g., Diongue et al. 2002). Therefore, the study will focus on the $D + 1$ forecast through the rest of the paper. This cannot replace a proper initialization of MCS-related features, but provides enough time for MCSs to develop within the simulation time window.

Another drawback of the forecasts is the lack of very low BT values. For example, in Fig. 2 (top), the BT minimum is 197 K in the observations and 214 K in the forecasts. Moreover, deep convective systems in the tropics are usually defined as pixels with BT less than the threshold of 230 K (e.g., Tian et al. 2004). Such pixels are much less numerous in the forecasts than in the observations. This discrepancy points out an underestimation of the convective updrafts and/or of the subgrid cloud fraction in the model. To alleviate this modeling drawback, cloud covers are defined hereafter as BT less than 260 K, which corresponds to high clouds (e.g., Fu et al. 1990; Tian et al. 2004). This threshold is suitable for tropical high clouds as it is close to the climatological temperature at 440 hPa. This tempera-

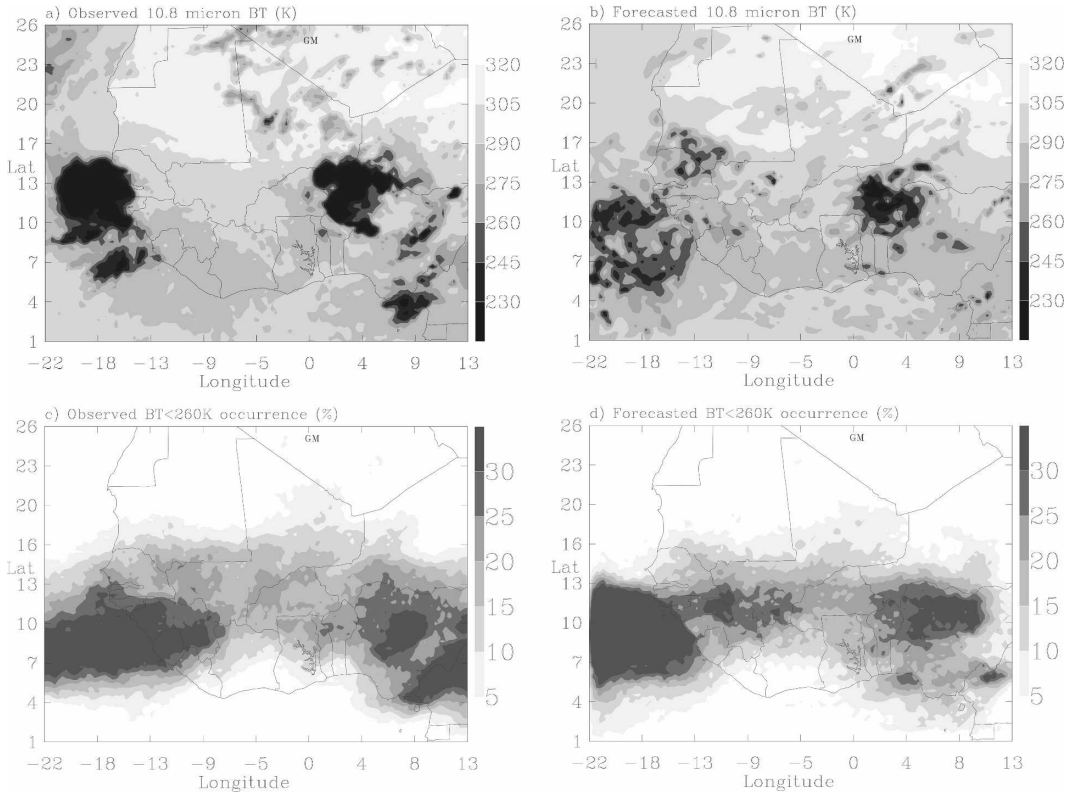


FIG. 2. (top) The 10.8-$\mu$m BT (K) at 1200 UTC 14 Aug 2006 and (bottom) occurrence (%) of high clouds during the 1-month period. Results are from (left) the MSG observation and (right) the Méso-NH forecast at $D + 1$.

ture threshold can detect deep convective clouds and cirrus anvil clouds, but may exclude some thin cirrus (Tian et al. 2004).

The occurrence of the high clouds during the 1-month period sampled every 3 h is shown in Fig. 2 (bottom). In the observation, the distribution shows a strong meridional organization with a maximum of high clouds between 5° and 15°N. The preferential locations of high clouds over the Jos Plateau and the Guinea Highlands indicate the influence of orography in triggering convection. This result is in agreement with a principal component analysis of the outgoing longwave radiation fluxes over Africa (Comer et al. 2007). Outside 5°–15°N, the domain is, on average, almost free of high clouds. A similar meridional organization of the high clouds can be seen in the forecast (Fig. 2d). However, their occurrence is overestimated at the western coasts and underestimated in the eastern boundaries of the domain. In the latter case, this is likely a boundary effect due to the coupling that used temperature, water vapor, and wind fields from ECMWF forecasts only. In the other case, the discrepancy may be partly attributed to the too-smooth orography described over the 32-km grid mesh, which leads to an underestimation of the orographic forcing. Between these two main orographic centers, the southern limit of high clouds is well delineated in the model but the occurrence of high clouds decreases more sharply than observed on the northern side of the maximum, in the Sahel.

The time evolution of the characteristics of the high clouds (i.e., cloud occupancy, number of cloud systems, and patchiness) is shown in Fig. 3. Observed high clouds present a diurnal cycle superimposed on lower-frequency variability. Particularly notable is the high-cloud peaking at a 25% maximum occupancy over the domain on 3 August, over values fluctuating around 5%–10%. This sharp intraseasonal maximum mostly occurs south of 10°N and coincides with a maximum of rainfall (not shown). The somewhat weaker but still obvious fluctuations taking place from 10 to 17 August concern variation of cloud cover in the 10°–15°N Sahelian band. In contrast to cloud occurrence, the number of observed cloud systems is less variable during the period with around 50 systems in the morning, a number that diminishes throughout the evening/night. The diurnal cycle of the observed patchiness is linked to the strong diurnal control on the timing of MCS formation that follows and emerges from the development of

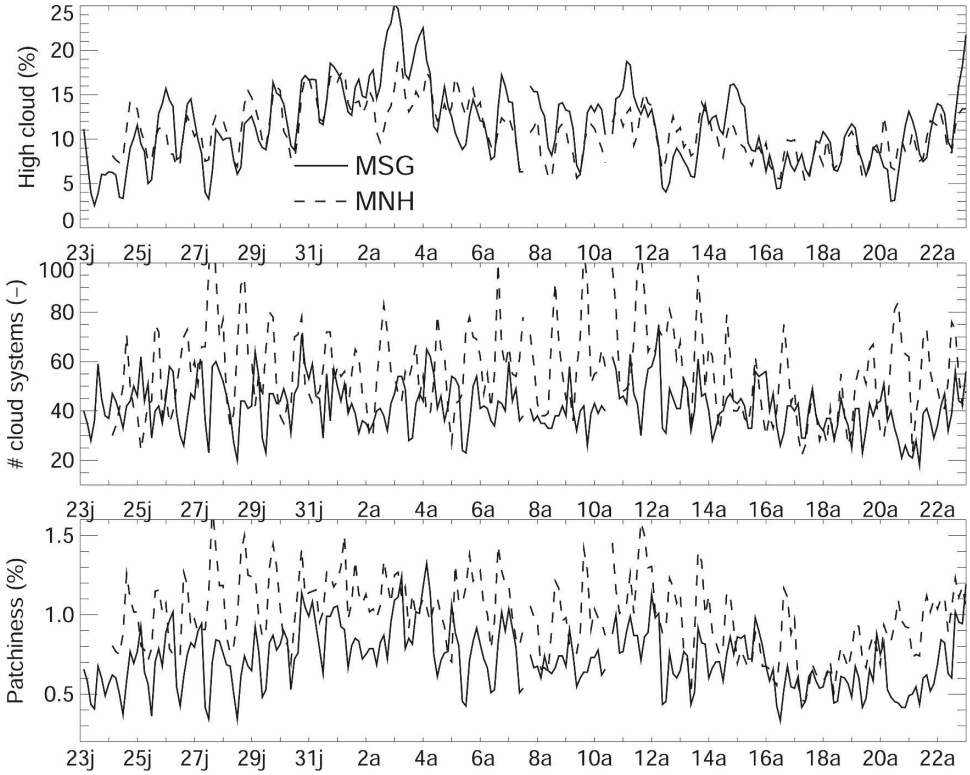


FIG. 3. Time evolution of cloud characteristics [i.e., high-cloud occupancy (%), number of cloud systems, and patchiness] from the MSG observation (solid) and the Méso-NH forecast (dashed) at $D$ + 1 over the simulation domain. The time axis is indicated by the day; July (J); August (A).

more patchy daytime convection. The forecasts mimic the low-frequency variability of the cloud characteristics reasonably well. On the other hand, large differences exist in the diurnal variation of the number of cloud systems. Too many cloud systems were forecasted in the afternoon. As the forecast number of high clouds was correct, the cloud systems were too patchy in the afternoon, indicating a lack of organized cloud systems in the forecasts.

Overall, the forecasted cloud features as presented in Fig. 3 appear to match a 30-day monsoon mean diurnal cycle too tightly each day. This is particularly true in the 10°–15°N band, where the forecasts do not properly account for the observed large-scale fluctuations of cloud occurrence, while they do reproduce quite well, albeit with a weaker amplitude, the early August episode of intraseasonal variability south of 10°N. This latitude-dependent performance may involve latitudinal changes in the characteristics of moist convection that cannot be captured by mesoscale simulations using current convection schemes.

The verification of the high-cloud forecasts over the domain was achieved using four categorical scores (POD, FAR, HSS, and FSS; Fig. 4). For the sake of clarity, only the POD and the FAR calculated over areas of 224 km by 224 km are shown. Indeed, the forecast presents a POD that is always lower than the FAR when compared grid point by grid point or over areas smaller than 224 km by 224 km (not shown), suggesting poor skill. However, the HSS values on a 32-km basis are low but positive. In consequence, the high-cloud forecasts can still be considered as useful since they are better than random chance.

When larger-sized areas are compared, the POD is around 0.6, generally over the FAR, around 0.4, when calculated over an area of 224 km by 224 km. So most of the high clouds were well forecasted at this scale, and a few were added or misplaced cloud forecasts. Consistently with POD and FAR results, a few days present lower HSS and FSS than the others. Also the FSS is always larger than $FSS_{random}$, indicating that the forecasts are more skillful than a random forecast (as already seen with POD and FAR). Interestingly, the HSS and the FSS increase with the area size. Over the largest area, these scores can even reach values around 0.6 and 0.8, respectively. This increase in skill with the area size is, however, somewhat artificial as it is larger for patchy than for organized cloud cover. This is confirmed with

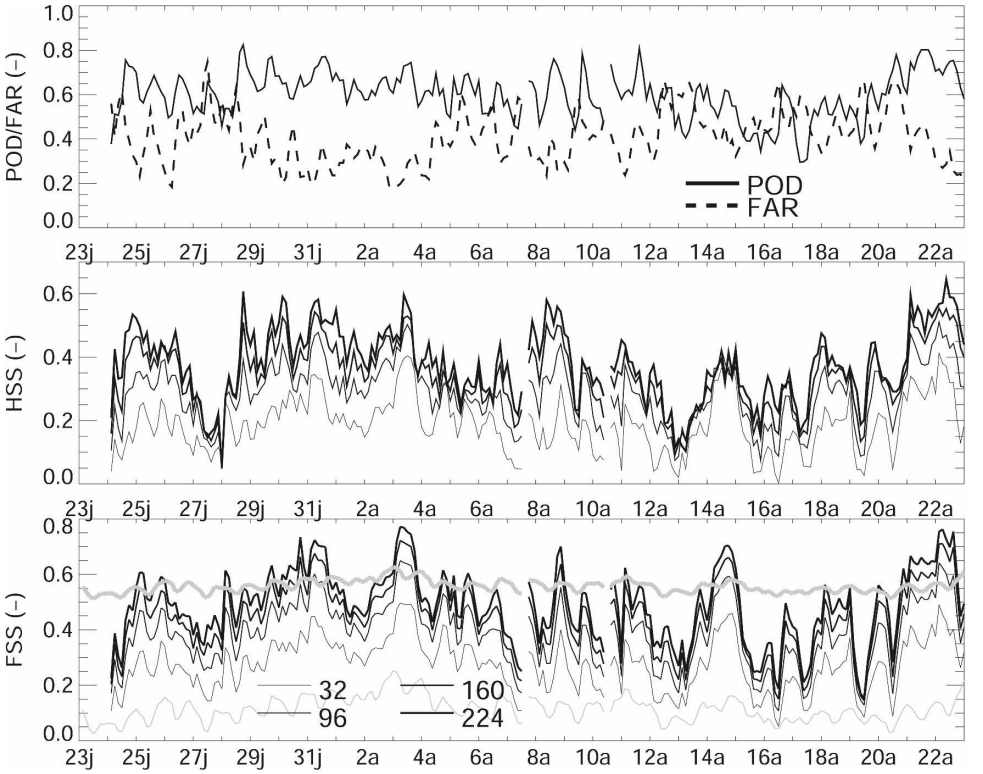


FIG. 4. Time evolution of categorical scores (i.e., POD, FAR, HSS, and FSS) over the simulation domain. The thicker the line, the larger the area on which the HSS and the FSS are calculated (from 32 km × 32 km to 224 km × 224 km). The POD and the FAR are shown from the 224 km × 224 km calculation only. (bottom) The thin (thick) gray line shows the $FSS_{random}$ ($FSS_{uniform}$).

the poorer skills obtained when calculating scores over latitudinal bands of 5°–10° and 10°–15°N.

The HSS and the FSS also present a diurnal variability, with a tendency to lower skill in the morning. This decrease in skill is due to MCSs that survive during the night. These MCSs are the most difficult to forecast as they result from the coupling of different processes including convection and dynamics. Furthermore, these scores show higher values at preferential periods a few days long, in particular when the FSS takes acceptable values (i.e., larger than $FSS_{uniform}$; for scales larger than 160 km). These variations are examined in the two following sections.

## 4. Diurnal variability

The West African monsoon is characterized by a meridional gradient in surface parameters that condition most of the climate variability with a strong diurnal cycle. The monsoon circulation is first examined both for the ECMWF analyses and the Méso-NH $D + 1$ forecasts using a classical latitude–altitude section of meteorological fields averaged over the whole period (Fig. 5).

In the analyses at 1200 UTC (Fig. 5a), the monsoon flow is characterized by large water vapor amounts in the first kilometer above ground level (AGL). For example, amounts larger than 15 g $kg^{-1}$ can be found up to 15°N within a mean southwesterly flow. The poleward advection of moist air favors the development of moist convection and cloud cover in the Sahelian band. In contrast, at latitudes higher than 20°N, the boundary layer is well developed over a 4-km depth as suggested by the weak isentropic gradient. Dry air with less than 10 g $kg^{-1}$ water vapor is transported by a mean northeasterly wind. Southward upward-sloping isentropes favor the export of dry Saharan (and sometimes dusty as observed during AMMA; Flamant et al. 2007) air up to 4 km equatorward, resulting in a layer referred to as the Saharan air layer (SAL). In the midtroposphere, the circulation is characterized by the so-called AEJ for which the well-defined core is located at 4 km AGL at 12°N. As the AEJ is close to thermal-wind balance, the jet core is associated with a baroclinic zone beneath it and isentropes sloping downward to the north. Overall, the ECMWF analyses at 1200 UTC correspond well to the vertical structure with latitude as recently analyzed from observed vertical profiles (Parker et al. 2005b)

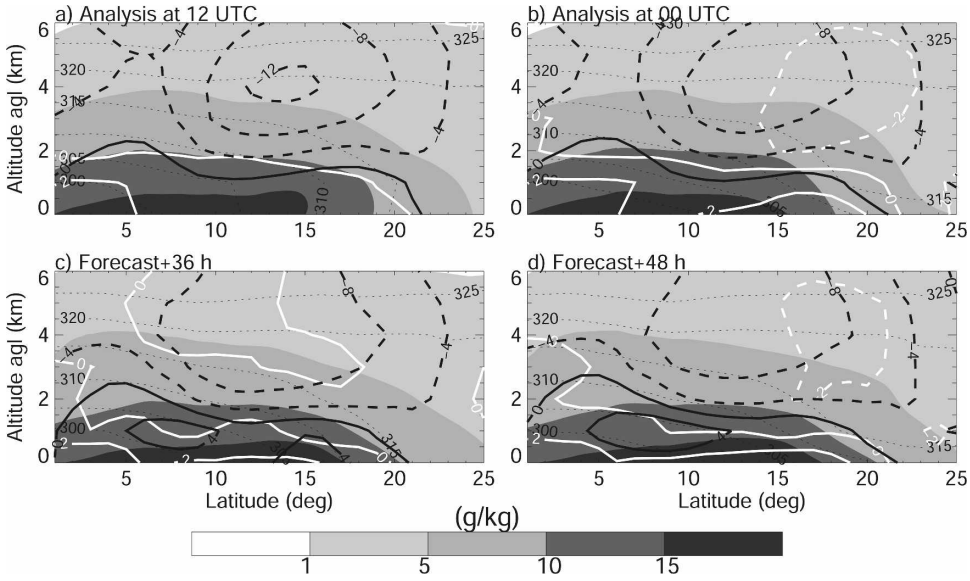


FIG. 5. Latitude–altitude section of the water vapor mixing ratio (g $kg^{-1}$) averaged over 10°W–10°E and over the whole period. Fields are taken from (a), (b) ECMWF analyses at 1200 and 0000 UTC and (c), (d) Méso-NH forecasts at +36 and +48 h. Thin dotted lines are isentropes every 5 K. Thick black (white) contours are zonal (meridional) winds every 4 (2) m $s^{-1}$ with solid (dashed) lines for positive (negative) values.

and using a two-dimensional numerical study (Peyrillé et al. 2007).

In the analyses at 0000 UTC (Fig. 5b), the nighttime cooling results in a stably stratified, less turbulent boundary layer. Then, the monsoon flux exhibits stronger southerly winds advecting moisture farther north at low levels. Above the southerlies, a well-marked northerly return flow lies around 4 km and 20°N. This clearly shows the meridional advection most efficient at night as already described with model analyses and observations by Parker et al. (2005a). Note also that the intensity of the AEJ core is reduced at night consistently with the decrease of the baroclinicity.

In the Méso-NH forecasts, the broad characteristics of the monsoon flux and the AEJ are well reproduced, as is their diurnal variation (Fig. 5, bottom). This is not unexpected as the model was not given enough time to develop any significant drift, in contrast to the disappearance of the AEJ after 5 days of forecast reported by Thorncroft et al. (2003). However, some departures from the analysis can be easily identified as shown below. They are representative of differences that built up during the course of each 48-h forecast. As such, they reveal some systematic drawbacks in the physical parameterizations when used together under environmental conditions that do not to depart too sharply from those observed. In practice, specific considerations led us to discard the first day (cf. the previous section).

The monsoon flow was faster than the analyses by a few meters per second both at 0000 and 1200 UTC. This faster monsoon flow is combined with a systematically shallower boundary layer. The surface signature of the forecasted intertropical discontinuity (ITD; the interface between the cool moist southwesterly monsoon flow and the warm, dry and aerosol-laden northeasterly harmattan flow) does not depart much from the one in the analysis. In contrast, the water vapor mixing ratio in the low-level monsoon flow does. In fact, north of 15°N, the meridional gradient of the forecasted low-level water vapor mixing ratio is shifted northward, as a shallow tongue of moist air is efficiently advected by the faster and thinner monsoon flow. The shallower boundary layer is consistent with these features: it promotes a low-level monsoon flow, which is less diluted in the vertical direction, thus limiting speed reduction and drying due to turbulent vertical mixing.

Farther south, associated with a larger isentropic gradient, a westerly jet located at 1 km AGL between 5° and 10°N was wrongly forecasted. In the free troposphere, the core of the AEJ was weaker and broader than in the analyses, and around 5°N, too strong easterlies were forecasted that may be related to the insufficient mixing in the shallow convection. The nighttime structure of the moisture field (after 48 h of simulation) is also striking: the depth of the layer with water vapor mixing ratio higher than 15 g $kg^{-1}$ steadily increases from the equator to the Sahel, in sharp contrast with the analysis, which indicates a thicker layer south of 10°N.

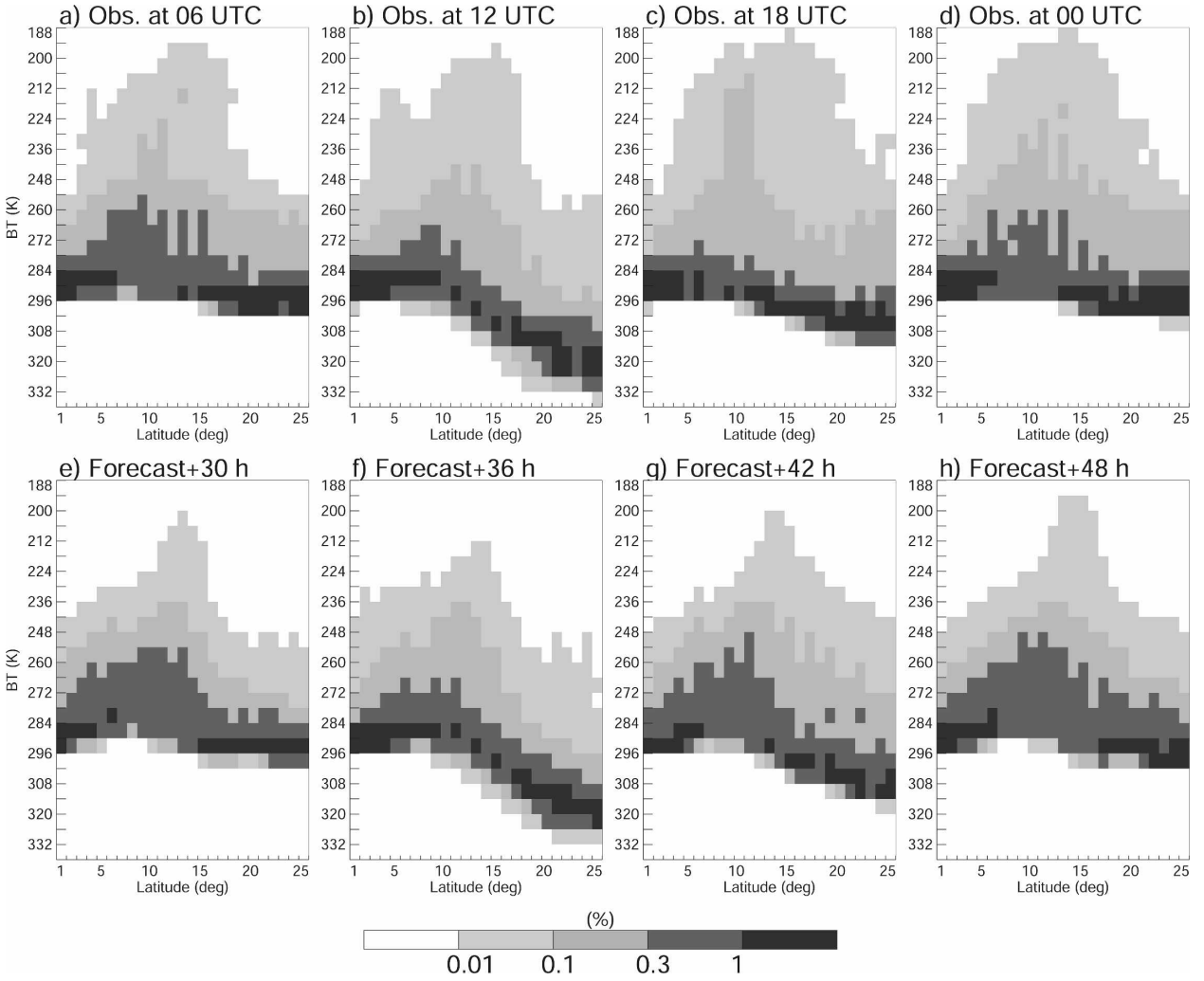


FIG. 6. Latitude–BT histograms over 10°W–10°E. Fields are taken from (a)–(d) MSG observations at 0600, 1200, 1800, and 0000 UTC and (e)–(h) Méso-NH forecasts at +30, +36, +42, and +48 h.

The accuracy of the analysis itself is expected to weaken at low levels because it is strongly controlled by the model physics there, even for locations where soundings are assimilated. Indeed, comparison of ECMWF analysis with available soundings across West Africa for this period suggests that the boundary layer is overall too deep in the analysis (not shown). Nevertheless, such discrepancies in the forecasts deserve further investigation. As we shall see in the next paragraph, at these lower latitudes, the model creates too many clouds at low levels. The latter inhibit the daytime boundary layer growth, a factor that probably plays a role in these large-scale circulation features.

The diurnal variability of the West African monsoon was further examined using histograms with latitude for the observed and forecast BTs averaged over 10°W–10°E every 6 h (Fig. 6). At 0600 UTC, the maximum observed BTs were around 290–296 K at latitudes less than 15°N and 296–302 K at higher latitudes. The meridional gradient in the BT maximum attains its climax at 1200 UTC. The southern coastline and the Sahara exhibit a 40-K difference with values of 290–296 and 332–340 K, respectively. This latitudinal variation results in the strong daytime heating that the deserts experience. In contrast, the larger heat capacity of the oceans and higher evaporative fraction of the tropical forests leads to almost no diurnal variation of the temperature at the surface and, hence, of the maximum BTs. With the decrease in the solar heating, the meridional gradient is greatly reduced at 1800 UTC. Between 0000 and 0600 UTC, the difference is minimum with a BT of 296 K over the Sahara due to strong nighttime cooling. Such diurnal variation in the BT maximum is well reproduced in the forecasts, but biased by a bin

width (6 K) between 5° and 10°N due to an overestimated low-cloud cover as explained next.

In the range of 260–290 K, observed BTs result in the presence of low-level and/or semitransparent ice clouds. Their occurrences at a maximum at 0000 and 0600 UTC and minimum at 1800 UTC. Chaboureau et al. (2007b) documented the diurnal cycle of cirrus over the same domain using a BT difference technique, but in late August 2005. They found a cirrus cover that was at a maximum at 1200 UTC. So the BT maximum in the 260–290-K range observed at 0000 UTC can be explained by an increase in the low-level clouds only. In contrast, the forecasted BTs in that range present a less marked diurnal cycle with an overestimation of their occurrence whatever the time. As the diurnal cycle of the cirrus cover is reasonably well forecasted by Méso-NH (Chaboureau and Pinty 2006; Chaboureau et al. 2007b), the discrepancy can be mainly attributed to an overestimation of the low-level cloud cover. Such low-level clouds are typically difficult to simulate with current parameterizations, regarding daytime as well as nighttime conditions (e.g., Lenderink et al. 2004; van Lipzig et al. 2006). The accuracy of surface sensible and latent heat fluxes is likely to play a role, too (e.g., Zhu and Albrecht 2003).

In the present case, from day 1 to day 2, there is an increase of the low-cloud cover that is associated with a decrease of the low-level temperature and of the lifting condensation level, together with a decrease of the equivalent potential temperature and CAPE; day 2 also follows an often rainy forecasted day 1 over 5°–10°N. This suggests a negative feedback loop between temperature and low-level clouds operating in the model over this area and at this time scale, involving cloud radiative properties, surface fluxes, and moist convection. An overall reduction in the rainfall occurs on day 2 compared to day 1 there, together with a CAPE decrease, while the opposite is found over the Sahel. Observations collected during the field campaign together with results from land surface modeling currently handled within AMMA will shed light on this issue. Besides, these variations of low-level temperature and of equivalent potential temperature lead to sharper meridional gradients over the continent, consistent with faster low-level winds.

The BTs less than 260 K occurred mostly between 5° and 15°N in both the observation and the forecast (as already seen in Fig. 2, bottom). The observed BTs in that range present a diurnal variability with a minimum at 1200 UTC and a maximum at 1800 UTC. The peak is typical of convection over land with a regime of deep convection in the afternoon (e.g., Nesbitt and Zipser 2003; Chaboureau et al. 2004). On the other hand the occurrence of observed BTs less than 230 K associated with deep convective clouds throughout the day is a signature of mesoscale convective systems that survive the night. Such low BTs were forecasted but with higher values. As noted earlier, this indicates a drawback in the representation of convective clouds in the model. Moreover BTs less than 230 K were correctly forecasted over 10°–15°N only. Indeed, the overestimation of low-level clouds between 5° and 10°N prevents boundary layer heating. Here, it leads to a decrease in CAPE and in the occurrence of deep convection as it is, by the construction of the convection scheme, strongly controlled by the CAPE.

## 5. Synoptic variability

The variability of the skill in forecasting high-cloud cover during the 1-month period is now examined. A large part of the variability during summer is due to traveling AEW of 3–5-day periods (Mekonnen et al. 2006). Figures 7a,b presents a Hovmöller diagram of the high-cloud cover and the 700-hPa meridional winds between 10° and 15°N taken from MSG observation and ECMWF analyses and forecasted by the Méso-NH model at $D + 1$ for the whole period. As illustrated in Fig. 7a, the cloud cover and meridional wind both display coherent and strong synoptic signatures, pointing to the significance of synoptic dynamics in shaping the cloud cover over West Africa. On the one hand, the presence of strong synoptic features can be thought of as a constraint that may benefit the forecast of cloud cover, at least at the larger synoptic scales. On the other hand, these features involve interactions across synoptic and mesoscales. Therefore, the answer also relies to some extent on the ability of the model to properly represent these scale interactions. Specific to our study though, the fact that we focus on short-term forecasts ($D + 1$) limits, in time, the impact of possible model weaknesses in the treatment of these complex phenomena.

In the observations, several cloud systems propagate westward ahead of an AEW trough. As in Berry and Thorncroft (2005) the term trough refers to the traveling coherent zero 700-hPa meridional wind. Many studies have shown that the region ahead of the AEW trough, where northerly flow both advects dry air equatorward and increases vertical shear, promotes the mesoscale organization of convective systems (e.g., Duvel 1990). For example, Fink and Reiner (2003) investigated the relationship between AEWs and squall lines over two extended summers. They found that the area west of the AEW trough was a favorable location for squall lines over the whole of tropical West Africa. In

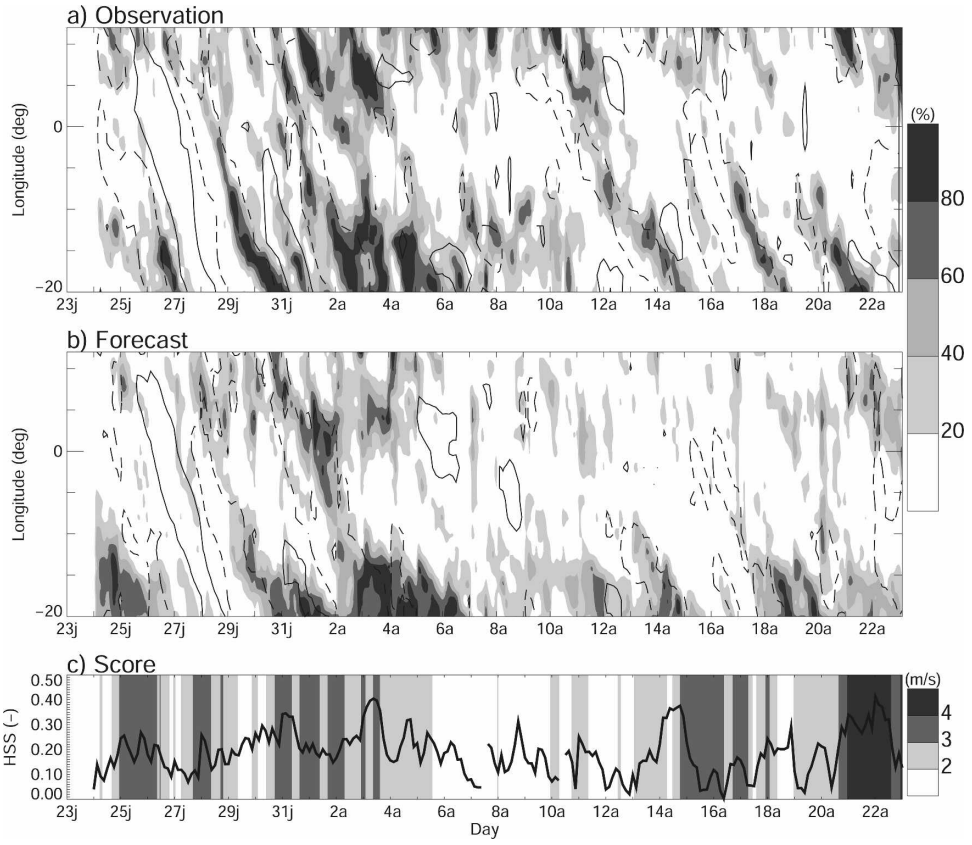


FIG. 7. (a), (b) Time–longitude diagram of wind and cloud fraction averaged between 10° and 15°N from 23 Jul to 22 Aug 2006: MSG cloud fraction (shading, %) and 700-hPa meridional wind contours at $-3$ m s$^{-1}$ (dashed) and at 3 m s$^{-1}$ (solid). Fields are taken from (a) MSG observations and ECMWF analyses and (b) Méso-NH forecasts at $D + 1$. (c) The time evolution of the HSS calculated point-by-point (line) and absolute meridional wind intensity from the analyses (shading, m s$^{-1}$) averaged over 10°–15°N.

the forecasts, as the cloud cover is patchier than observed, the organization of cloud systems as propagating lines appears less dramatic, albeit present. Another source of difference is the simulated dynamics: the meridional wind intensity in the forecasts shows weaker AEW activity than the analysis does.

The outlines of the AEW activity over the 1-month period are shown with the time evolution of the absolute meridional wind intensity from the analyses (Fig. 7c). It can be defined by two periods of enhanced AEW activity (the last week of July and the last two weeks of August) separated by an inactive week-long period around mid-August. Overall, the HSS tends to show higher skill forecasts during the active periods, particularly on 25–26 July, 31 July, and 21–22 August. The case of 14 August shown as an example in Fig. 2 (top) was obviously chosen because of its high skill. On 16 August, the poor skill is due to failure to forecast a cloud system observed ahead of a trough.

The relationship between HSS and absolute meridional wind is further explored with a scatterplot (Fig. 8). The correlation coefficient is 0.36. It further reduces to 0.27 when considering HSS calculated over areas of 224 km by 224 km. (The decrease in the correlation for larger areas suggests less sensitivity of the skill scores to dynamics when they are calculated over larger scales. The larger the area over which the score is calculated, the lower the fraction of the error at smaller scales that is due to displacement of the cloud entities.) A high correlation is not a priori expected given the complex chain of process interactions that give rise to the observed BTs. This result, however, suggests that the synoptic forcing during phases of AEW activity indeed increases the forecast skill. Note also that the increase of HSS is not related to an increase in cloud cover as HSS was conceived as an equitable score (Wilks 1995). By standardizing so that random forecasts have zero skill, HSS is a useful statistic for forecasts of variable events with time. As random forecasts vary with the number of forecasted and observed events, we effectively found

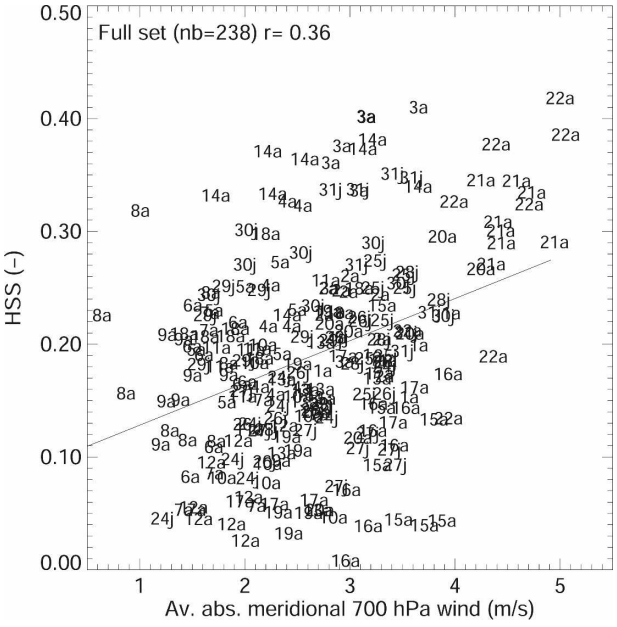


FIG. 8. Scatterplot between HSS and average absolute meridional 700-hPa wind calculated between 10° and 15°N from ECMWF analyses. The characters indicate the day; July (j); August (a).

that HSS and high-cloud cover (either forecasted or observed) were not correlated. Indeed, a higher value of HSS indicates a better forecast.

From a broader perspective, a large part of the high-cloud cover is linked to moist deep convection. This suggests that relationships between the cloud cover and AEWs may be influenced by the convection scheme, in particular by its closure. For instance, a closure based on moisture convergence (e.g., Bougeault 1985) may lead to convection being more constrained by the model dynamics, while a CAPE closure—as used here—will be more sensitive to changes in the magnitude of the local atmospheric instability. This issue requires further investigation.

## 6. Conclusions

During summer 2006, 2-day forecasts were performed daily over a domain covering West Africa with a 32-km grid mesh. The 3-hourly forecasts of cloud cover were verified by comparison with MSG observations at 10.8 $\mu$m. The verification was based on the model-to-satellite approach that consists of a direct comparison between observed and forecasted BTs. Combined with the calculation of scores, the approach is shown to be worthwhile, especially over data-sparse regions such as the tropics, in giving an objective evaluation of the representation of clouds in the model and in measuring the skill of cloud forecasts.

The West African monsoon is characterized by a strong meridional contrast in surface properties. Moist air is advected poleward up to 15°N yielding a maximum of cloud cover between 5° and 15°N while a deep boundary layer develops beyond 20°N. These broad characteristics of the West African monsoon are well reproduced by the forecasts. The diurnal variation of the 10.8-$\mu$m BTs with latitude is also well captured, in particular the meridional contrast of clear-sky BTs, maximum at 1200 UTC, and the occurrence of low BTs, maximum at 1800 UTC. This is consistent with the monsoon circulation as described by the ECMWF analyses and forecasted by the model: the low-level monsoon flux increases with the nighttime boundary layer stratification while the AEJ increases with the solar heating. Such good performance shows at the very least the progress made in the surface field analysis since the pioneering work of Morcrette (1991).

Some systematic errors in representing clouds were, however, identified. First, the lack of cloud systems predicted in the morning of the first day led the study to focus on the $D + 1$ forecasts. This is linked to the use of a cold start but also to the specific nature of the phenomena define the cloud cover. Typically MCSs contribute significantly to the signal and are characterized by time scales much larger than a few hours. Then the occurrence of forecasted BTs less than 230 K associated with deep convective clouds is greatly underestimated. This obliges us to address the verification of high-cloud cover (i.e., deep convection and cirrus anvil clouds as defined by BTs less 260 K). As a result, the high-cloud cover is found to be well represented in number but too patchy. Too many low-level clouds were also found between 5° and 10°N. This causes a less-developed boundary layer during daytime resulting in too strong a monsoon flux at the low level.

The systematic errors highlighted by the cloud cover verification pinpoint several modeling drawbacks. The lack of low BTs can be explained by an underestimation of the convective updrafts and/or of the subgrid cloud fraction in the model. It is also partly due to an overestimation of low-level clouds between 5° and 15°N. This requires further work on the convection scheme, for both triggering and entrainment, as well as the subgrid cloud scheme. Such a feature may be at least partly explained by too small values of daytime low-level equivalent potential temperature associated with the radiative impact of the too large low-level cloud cover. The approach developed here affords an ideal framework for such developments on cloud parameterizations. Also, some of the forecast errors are due to dis-

crepancies in the initial fields. The use of reanalyses or analyses from other forecast systems would allow the sensitivity of the forecast errors to the initial conditions to be tested. The impact of nudging with satellite observations should also be explored in the aim of overcoming the limitations imposed by a cold start.

Finally, the variation of the HSS with time over the 1-month period was examined together with the variation of the 700-hPa meridional wind. It showed a general increase of the skill with the AEW activity. This result, albeit fragile, points out the role of the synoptic regimes on the accuracy of the forecast. The method of verification developed here allows us to suggest such a relationship. In consequence, a better analysis of the atmospheric flow would have a positive impact on operational forecasts of mesoscale convective systems during periods of wave activity. This result provides additional motivation for building an observation system that covers West Africa well.

*Acknowledgments.* Based on a French initiative, AMMA was built by an international scientific group and is currently funded by a large number of agencies, especially from France, the United Kingdom, the United States, and Africa. It has been the beneficiary of a major financial contribution from the European Community's Sixth Framework Research Programme. Detailed information on scientific coordination and funding is available on the AMMA International Web site (http://www.amma-international.org). Nathalie Söhne was supported by a CNES and Météo-France Ph.D. grant. Computer resources were allocated by IDRIS. MSG observations were obtained from Météo-France/Centre de Météorologie Spatiale. The authors thank Nicole Asencio and Fleur Couvreux for useful discussions concerning modeling aspects.

## REFERENCES

Adler, R. F., C. Kidd, G. Petty, M. Morissey, and H. M. Goodman, 2001: Intercomparison of global precipitation products: The Third Precipitation Intercomparison Project (PIP-3). *Bull. Amer. Meteor. Soc.,* **82,** 1377–1396.

Bechtold, P., E. Bazile, F. Guichard, P. Mascart, and E. Richard, 2001: A mass flux convection scheme for regional and global models. *Quart. J. Roy. Meteor. Soc.,* **127,** 869–886.

Berry, G. J., and G. Thorncroft, 2005: Case study of an intense African easterly wave. *Mon. Wea. Rev.,* **133,** 752–766.

Bougeault, P., 1985: A simple parameterization of the large-scale effects of cumulus convection. *Mon. Wea. Rev.,* **113,** 2108–2121.

Burpee, R. W., 1972: The origin and structure of easterly waves in the lower troposphere of North Africa. *J. Atmos. Sci.,* **29,** 77–90.

Chaboureau, J.-P., and P. Bechtold, 2002: A simple cloud parameterization derived from cloud resolving model data: Diagnostic and prognostic applications. *J. Atmos. Sci.,* **59,** 2362–2372.

——, and ——, 2005: Statistical representation of clouds in a regional model and the impact on the diurnal cycle of convection during Tropical Convection, Cirrus and Nitrogen Oxides (TROCCINOX). *J. Geophys. Res.,* **110,** D17103, doi:10.1029/2004JD005645.

——, and J.-P. Pinty, 2006: Evaluation of a cirrus parameterization with Meteosat Second Generation. *Geophys. Res. Lett.,* **33,** L03815, doi:10.1029/2005GL024725.

——, J.-P. Cammas, P. Mascart, J.-P. Pinty, C. Claud, R. Roca, and J.-J. Morcrette, 2000: Evaluation of a cloud system life-cycle simulated by Meso-NH during FASTEX using METEOSAT radiances and TOVS-3I cloud retrievals. *Quart. J. Roy. Meteor. Soc.,* **126,** 1735–1750.

——, ——, ——, ——, and J.-P. Lafore, 2002: Mesoscale model cloud scheme assessment using satellite observations. *J. Geophys. Res.,* **107,** 4301, doi:10.1029/2001JD000714.

——, F. Guichard, J.-L. Redelsperger, and J.-P. Lafore, 2004: The role of stability and moisture in the development of convection. *Quart. J. Roy. Meteor. Soc.,* **130,** 3105–3117.

——, J.-P. Cammas, J. Duron, P. J. Mascart, N. M. Sitnikov, and H.-J. Voessing, 2007a: A numerical study of tropical cross-tropopause transport by convective overshoots. *Atmos. Chem. Phys.,* **7,** 1731–1740.

——, P. Tulet, and C. Mari, 2007b: Diurnal cycle of dust and cirrus over West Africa as seen from Meteosat Second Generation satellite and a regional forecast model. *Geophys. Res. Lett.,* **34,** L02822, doi:10.1029/2006GL027771.

——, and Coauthors, 2008: A midlatitude precipitating cloud database validated with satellite observations. *J. Appl. Meteor. Climatol.,* **47,** 1337–1353.

Chevallier, F., and G. Kelly, 2002: Model clouds as seen from space: Comparison with geostationary imagery in the 11-$\mu$m window channel. *Mon. Wea. Rev.,* **130,** 712–722.

Comer, R. E., A. Slingo, and R. P. Allan, 2007: Observations of the diurnal cycle of outgoing longwave radiation from the Geostationary Earth Radiation Budget instrument. *Geophys. Res. Lett.,* **34,** L02823, doi:10.1029/2006GL028229.

Diedhiou, A., S. Janicot, A. Viltard, P. de Felice, and H. Laurent, 1999: Easterly wave regimes and associated convection over West Africa and tropical Atlantic: Results from the NCEP/NCAR and ECMWF reanalyses. *Climate Dyn.,* **15,** 795–822.

Diongue, A., J.-P. Lafore, J.-L. Redelsperger, and R. Roca, 2002: Numerical study of a Sahelian synoptic weather system: Initiation and mature stages of convection and its interactions with the large-scale dynamics. *Quart. J. Roy. Meteor. Soc.,* **128,** 1899–1927.

Duvel, J. P., 1990: Convection over tropical Africa and the Atlantic Ocean during northern summer. Part II: Modulation by easterly waves. *Mon. Wea. Rev.,* **118,** 1855–1868.

Ebert, E. E., U. Damrath, W. Wergen, and M. E. Baldwin, 2003: The WGNE assessment of short-term quantitative precipitation forecasts. *Bull. Amer. Meteor. Soc.,* **84,** 481–492.

Fink, A. H., and A. Reiner, 2003: Spatiotemporal variability of the relation between African Easterly Waves and West African Squall Lines in 1998 and 1999. *J. Geophys. Res.,* **108,** 4332, doi:10.1029/2002JD002816.

Finley, J. P., 1884: Tornado predictions. *Amer. Meteor. J.,* **1,** 85–88.

Flamant, C., J.-P. Chaboureau, D. J. Parker, C. M. Taylor, J.-P. Cammas, O. Bock, F. Timouk, and J. Pelon, 2007: Airborne observations of the impact of a convective system on the

planetary boundary layer thermodynamics and aerosol distribution in the inter-tropical discontinuity region of the West African Monsoon. *Quart. J. Roy. Meteor. Soc.,* **133,** 1175–1189.

Fu, R., A. D. Del Genio, and W. B. Rossow, 1990: Behavior of deep convective clouds in the tropical Pacific deduced from ISCCP radiances. *J. Climate,* **3,** 1129–1152.

Guichard, F., and Coauthors, 2004: Modelling the diurnal cycle of deep precipitating convection over land with cloud-resolving models and single-column models. *Quart. J. Roy. Meteor. Soc.,* **130,** 3139–3172.

Hall, N. M. J., G. N. Kiladis, and C. D. Thorncroft, 2006: Three dimensional structure and dynamics of African easterly waves. Part II: Dynamical modes. *J. Atmos. Sci.,* **63,** 2231–2245.

Hsieh, J.-S., and K. H. Cook, 2005: Generation of African easterly wave disturbances: Relationship to the African easterly jet. *Mon. Wea. Rev.,* **133,** 1311–1327.

Kain, J. S., and J. M. Fritsch, 1993: Convective parameterization for mesoscale models: The Kain-Fritsch Scheme. *The Representation of Cumulus Convection in Numerical Models, Meteor. Monogr.,* No. 46, Amer. Meteor. Soc., 165–170.

Keil, C., A. Tafferner, and T. Reinhardt, 2006: Synthetic satellite imagery in the Lokal-Modell. *Atmos. Res.,* **82,** 19–25.

Lafore, J.-P., and Coauthors, 1998: The Meso-NH Atmospheric Simulation System. Part I: Adiabatic formulation and control simulations. Scientific objectives and experimental design. *Ann. Geophys.,* **16,** 90–109.

Lebel, T., F. Delclaux, L. Le Barb, and J. Polcher, 2000: From GCM scales to hydrological scales: Rainfall variability in West Africa. *Stoch. Environ. Res. Risk Assess.,* **14,** 275–295.

Lenderink, G., and Coauthors, 2004: The diurnal cycle of shallow cumulus clouds over land: A single-column model intercomparison study. *Quart. J. Roy. Meteor. Soc.,* **130,** 3339–3364.

Mari, C., and Coauthors, 2006: Regional lightning NOx sources during the TROCCINOX experiment. *Atmos. Chem. Phys.,* **6,** 5559–5572.

Mathon, V., H. Laurent, and T. Lebel, 2002: Mesoscale convective system rainfall in the Sahel. *J. Appl. Meteor.,* **41,** 1081–1092.

Mekonnen, A., C. D. Thorncroft, and A. R. Aiyyer, 2006: Analysis of convection and its association with African easterly waves. *J. Climate,* **19,** 5405–5421.

Morcrette, J.-J., 1991: Evaluation of model-generated cloudiness: Satellite-observed and model-generated diurnal variability of brightness temperature. *Mon. Wea. Rev.,* **119,** 1205–1224.

Nesbitt, S. W., and E. J. Zipser, 2003: The diurnal cycle of rainfall and convective intensity according to three years of TRMM measurements. *J. Climate,* **16,** 1456–1475.

Parker, D. J., and Coauthors, 2005a: The diurnal cycle of the West African monsoon circulation. *Quart. J. Roy. Meteor. Soc.,* **131,** 2839–2860.

——, C. D. Thorncroft, R. R. Burton, and A. Diongue-Niang, 2005b: Analysis of the African easterly jet, using aircraft observations from the JET2000 experiment. *Quart. J. Roy. Meteor. Soc.,* **131,** 1461–1482.

Peyrillé, P., J.-P. Lafore, and J.-L. Redelsperger, 2007: An idealized two-dimensional framework to study the West African monsoon. Part I: Validation and key controlling factors. *J. Atmos. Sci.,* **64,** 2765–2782.

Pinty, J.-P., and P. Jabouille, 1998: A mixed-phase cloud parameterization for use in a mesoscale non-hydrostatic model: Simulations of a squall line and of orographic precipitations. Preprints, *Conf. on Cloud Physics,* Everett, WA, Amer. Meteor. Soc., 217–220.

Redelsperger, J.-L., C. D. Thorncroft, A. Diedhiou, T. Lebel, D. J. Parker, and J. Polcher, 2006: African Monsoon Multidisciplinary Analysis: An international research project and field campaign. *Bull. Amer. Meteor. Soc.,* **87,** 1739–1746.

Reed, R. J., D. C. Norquist, and E. E. Recker, 1977: The structure and properties of African wave disturbances as observed during phase III of GATE. *Mon. Wea. Rev.,* **105,** 317–333.

Roberts, N. M., and H. W. Lean, 2008: Scale-selective verification of rainfall accumulations from high-resolution forecasts of convective events. *Mon. Wea. Rev.,* **136,** 78–97.

Saunders, R., M. Matricardi, P. Brunel, S. English, P. Bauer, U. O'Keeffe, P. Francis, and P. Rayer, 2005: RTTOV-8 Science and validation report. NWP SAF Rep., Tech. Rep., 41 pp.

Schröder, M., and Coauthors, 2006: Comparison of model predicted low-level cloud parameters with satellite remote sensing observations during two days of the BALTEX Bridge campaigns. *Atmos. Res.,* **82,** 83–101.

Simmons, A. J., and A. Hollingsworth, 2002: Some aspects of the improvement in skill of numerical weather prediction. *Quart. J. Roy. Meteor. Soc.,* **128,** 647–677.

Smith, R. K., G. Garden, J. Molinari, and B. R. Morton, 2001: Proceedings of an international workshop on the dynamics and forecasting of tropical weather systems. *Bull. Amer. Meteor. Soc.,* **82,** 2825–2829.

Söhne, N., J.-P. Chaboureau, S. Argence, D. Lambert, and E. Richard, 2006: Objective evaluation of mesoscale simulations of the Algiers 2001 flash flood by the model-to-satellite approach. *Adv. Geosci.,* **7,** 247–250.

Taylor, C. M., and R. J. Ellis, 2006: Satellite detection of soil moisture impacts on convection at the mesoscale. *Geophys. Res. Lett.,* **33,** L03404, doi:10.1029/2005GL025252.

Thorncroft, C. D., and Coauthors, 2003: The JET2000 Project: Aircraft observations of the African easterly jet and African easterly waves. *Bull. Amer. Meteor. Soc.,* **84,** 337–351.

Tian, B., B. J. Soden, and X. Wu, 2004: Diurnal cycle of convection, clouds, and water vapor in the tropical upper troposphere: Satellites versus a general circulation model. *J. Geophys. Res.,* **109,** D10101, doi:10.1029/2003JD004117.

Tompkins, A. M., C. Cardinali, J.-J. Morcrette, and M. Rodwell, 2005: Influence of aerosol climatology on forecasts of the African Easterly Jet. *Geophys. Res. Lett.,* **32,** L10801, doi:10.1029/2004GL022189.

van Lipzig, N., and Coauthors, 2006: Comparison of model predicted low-level cloud parameters with observations from the BALTEX Bridge Campaign cases. *Atmos. Res.,* **82,** 55–82.

Wilks, D. S., 1995: *Statistical Methods in the Atmospheric Sciences.* Academic Press, 467 pp.

Zhu, P., and B. Albrecht, 2003: Large eddy simulations of continental shallow cumulus convection. *J. Geophys. Res.,* **108,** 4453, doi:10.1029/2002JD003119.